Geophys. J. R. astr. Soc. (1978) **53**, 559–581

Measurements and interpretation of normal mode attenuation

Richard V. Sailor and Adam M. Dziewonski *Department of Geological Sciences, Harvard University, Cambridge, Massachusetts 02138, USA*

Received 1977 November 2; in original form 1977 June 28

Summary. Measurements of Q for modes of free oscillation provide the most accurate information about the anelastic properties of the whole Earth in the period range from 100 to 3000 s. We have obtained more than 230 Q measurements, by using two different techniques. Individual LaCoste–Romberg gravimeter recordings of three large earthquakes were used to observe the time rate of decay of spectral peaks corresponding to different modes. This method provided measurements of Q for 37 different modes. By stacking 211 WWSSN recordings of two deep earthquakes, we were able to measure Q for 197 modes, including many overtones which cannot be analysed using the spectra of individual recordings.

We inverted these data to obtain models of the distribution of Q in the mantle. Inversion in the data space can provide smooth models of the variation of Q in the mantle, without being subject to the bias of pre-conceived model parameterization. The data-space inversion experiments gave no indication of large variations of Q in the lower mantle, and provided an indication of the resolution attained by our data. We show that the data are consistent with very simple Q models of the mantle. The data for modes dominated by shear energy can be satisfied by models with constant Q_μ^{-1} (attenuation of shear energy) in two regions: the upper mantle in which Q_μ is about 110, and the lower mantle below 670 km, in which Q_μ is a little below 400. The average Q_μ of the mantle is about 210. Models in which only shear energy is dissipated do not satisfy our observations of Q for radial modes. We infer that there is a zone within the Earth with a non-zero Q_K^{-1} (bulk dissipation). All the data are satisfied with Q_K of approximately 400 in the upper mantle. In that case, $\bar{Q}_{ScS} \sim 230$.

1 Introduction

The accurate determination of the anelastic properties of the Earth is beoming increasingly important. Since anelastic behaviour, as manifested by the attenuation of seismic energy, is physically connected with such properties as temperature, viscosity, and the amount of partial melting, studies of anelastic behaviour will provide important information about the

Earth's interior. Furthermore, the existence of any amount of anelastic dissipation requires that there be a dependence of elastic properties (such as body-wave velocities) on frequency. The implications of this anelastic velocity dispersion are of great importance to seismology.

It has recently been shown that the dispersion caused by the Earth's anelasticity is large enough that it should be taken into account in the construction of earth models. Akopyan, Zharkov & Lyubimov (1975, 1976); Liu, Anderson & Kanamori (1976) and Hart, Anderson & Kanamori (1977) have approached the problem by 'correcting' the observed eigenperiods for attenuation before performing inversion to find an earth model. The resulting earth model is said to be comparable with the velocity models derived using short-period body waves. This procedure can eliminate the 'base-line' problem – the problem that travel times predicted by earth models derived from free oscillations are generally slower than those predicted by earth models derived from body waves. Lee & Solomon (1978), in a study of surface waves, have shown that it is strictly more correct to perform simultaneous inversion for elastic and anelastic properties, rather than 'correcting' some of the observations. Dziewonski (1977) has used the simultaneous inversion approach to obtain both elastic and anelastic parameters of an earth model which is consistent with a large set of free oscillation and body-wave data.

At the present time, elastic earth models derived from body waves and free oscillations have become quite refined, while the anelastic properties of the Earth are still very poorly resolved. This is because attenuation measurements are easily biased by extraneous factors, and hence the corresponding values from different studies may vary greatly. Measurements of Q for modes of free oscillation have been reported by Benioff, Press & Smith (1961); Ness, Harrison & Slichter (1961); Alsop, Sutton & Ewing (1961); MacDonald & Ness (1961); Smith (1961, 1972); Slichter (1967a,b); Nowroozi (1968, 1974); Dratler *et al.* (1971); Gaulon (1971); Reiter (1973); Roult (1974, 1975); Jobert & Roult (1976) and Buland & Gilbert (1977). There is great scatter among the values given in these reports, and as Smith (1972) indicated in his review of the anelasticity of the mantle, this is what has discouraged extensive inversion studies of attenuation data. Indeed, previous inversion studies have shown the inconsistency and poor resolution of such data (Jackson 1971; Deschamps 1977).

The purpose of this paper is to provide a better description of the anelastic properties of the average earth. As a first approximation, we can consider the anelastic properties separately, without taking into account the coupling to elastic properties. And, in spite of the known lateral heterogeneity of both elastic and anelastic properties of the Earth, it will still be useful to consider the concept of a spherically symmetric average earth. The average earth can serve as a standard of comparison for seismic observations made in more limited regions.

Since observations of free oscillations have been very successfully used in the development of elastic average-earth models, it is reasonable to expect that they also may be used to develop a model of average-earth attenuation. But until recently, this has not been possible because Q measurements could be obtained only for a relatively small number of modes – those which are above the noise level on individual recordings. However, the method of phase equalization or 'stacking' dramatically improves the signal to noise ratio by allowing the data from many recordings to be used simultaneously, when the earthquake source mechanism is known (Mendiguren 1973; Gilbert & Dziewonski 1975). In this paper we will show how this technique may be used to measure Q for a relatively large number of modes, including many overtones. We have also measured Q by a more traditional method, using individual gravimeter recordings. This body of data may be inverted to derive simple models of the distribution of Q in the mantle.

2 Data

In this study, we used two different sets of seismic data, and two different techniques for measuring Q of modes of free oscillation. The first subset of the data consists of four gravimeter recordings of three large earthquakes. The second part of the data is a set of 211 WWSSN recordings of two deep earthquakes. Stacking was used to measure Q from the WWSSN recordings, while a much simpler method, involving the time decay of a spectral peak, was applied to the gravimeter recordings.

The three events for which we had time series recorded by LaCoste gravimeters are: the 1964 Alaskan, 1970 Colombian and the 1975 Solomon Islands earthquakes. The Colombian earthquake occurred at a depth of 650 km with a magnitude of 7.1 (m_b). Dratler *et al.* (1971) noted that this earthquake strongly excited several high-Q modes, and they listed the periods and observed Q of these modes. We have re-examined this same LaCoste recording, which is from the station at Payson, Arizona. Our measured Q values are in general agreement with those reported by Dratler *et al.* However, a change in convention of mode identification requires that several of these modes be reclassified. Changes of identification are indicated in Table 1.

Further information on this recording of the July 31 Colombia earthquake is as follows: total duration: 67 hr 13 min; sampling interval: 12 s; starting time of recording: 8 hr 52 min; end of recording: 76 hr 5 min.

The 1964 March 31 Alaska earthquake was recorded by two LaCoste gravimeters (designated as #4 and #7) at UCLA. The original, unprocessed data were generously provided by Professor L. B. Slichter, who has described it previously (Slichter 1967a, b). These unique recordings have a total duration of 18 day, 12 hr and 28 min and were recorded at the rate of 1 sample per minute.

There was a significant number of large amplitude glitches left after the records were detrended and the 20 most significant tides removed by least-squares fit. Wiggins & Miller (1972) have processed the record from gravimeter #4 using a prediction error filter. Most of the glitches can be easily identified by visual inspection. Also, we know that the signal in the recording represents a superposition of normal modes. Thus, a simpler approach seemed preferable. We have adopted the following procedure:

(1) The noisy segments of the time series (3–5 per cent of the total length of the recordings) were filled with zeros.
(2) The spectrum of this processed record was bandpass filtered through a system of filters centred about the eigenfrequencies of well-excited normal modes (only the modes with periods greater than 500 s were considered).
(3) The segments of the time series obtained by the inverse FFT of the spectrum processed in step (2) were substituted into the noisy parts of the original recording.

Most of our work was done with the recording of gravimeter #4 which is less noisy. Slichter (1967b) indicated that gravimeter #7 has a systematically lower response at higher frequencies, due to its higher gear ratio in the servo system.

The 1975 July 20 Solomon Islands earthquake had a focal depth of 49 km and $M_s = 7.5$ (BRK), according to the PDE catalogue. Our time series was recorded at the rate of three samples per minute on the LaCoste gravimeter located at Naña, Peru. The record analysed began 1 hr 44 min after the origin time and extended for a total of 70 hr.

For stacking, the data set is the same as that used by Gilbert & Dziewonski (1975) and Dziewonski & Gilbert (1974). This consists of 165 long-period recordings of the 1970 Colombia earthquake (from 65 different WWSSN stations), and 46 recordings (from 35 different stations) of the 1963 August 15 Peru–Bolivia earthquake. The details involving

the stations and components used, and the initial data processing, are given by Gilbert & Dziewonski (1975, Section 3.1).

The 165 recordings of the Colombia earthquake have an average length of about 18 hr. The maximum time window formed by overlapping these records is approximately 48 hr, beginning 17 min after the origin time.

The 46 recordings of the Peru–Bolivia earthquake average about 12 hr in length and cover a maximum time window about 35 hr long, starting 10 min after the origin time.

3 *Q* observations

3.1 SINGLE RECORDINGS

To measure values of Q from the four gravimeter recordings, we have used the technique of observing the time rate of decay of an individual peak in the amplitude spectrum (*cf.* Ness *et al.* 1961). We determine the mean energy of a particular spectral peak in successive time intervals or windows. A plot of the log of the mean energy (or the power in dB) versus the mid-point of the corresponding time interval will define a straight line with slope proportional to $1/QT$, where T is the period of the oscillation. From a least-squares line fit, we find $1/Q$ and the standard deviation of $1/Q$.

Splitting of the normal modes may lead to erroneous results if this traditional technique is applied incorrectly. Alsop, Sutton & Ewing (1961) have discussed this problem in detail. They noted three criteria, at least one of which must be satisfied in order that the method should yield acceptable answers. If the Earth's rotation were the only cause for splitting, all our measurements satisfy the appropriate conditions. The case of splitting due to lateral heterogeneities (including ellipticity) still needs to be studied. However, the internal consistency of our data indicates that the errors due to splitting of spectral lines are not very large, as the errors should be random for different modes of the same overtone branch (fundamental spheroidal mode, for example). The effect of splitting on measurements of Q of normal modes has also been considered by Stein & Geller (1977).

For our Q measurements we tried several different window lengths. For ${}_0S_0$ and ${}_0S_2$ we used six-day windows offset by one day (i.e. segments of the time series from 0 to 6 day, 1 to 7 day, etc.), and one-day non-overlapping windows. But the shorter period modes with lower Q decay down to the noise level more quickly, and shorter windows must be used. Other windows used in this study were: a four-day window shifted in steps of 1/2 day; a 30 hr window shifted in steps of 15 hr, and 20 hr windows shifted by 10 hr.

The central frequency and the shape of some spectral peaks may tend to change slightly among the different windowed spectra. The maximum power of a given peak followed through successive windows then does not decay as stably as the 'average power' of the peak, which may be determined by integrating across the central part of the peak. The 'average power', $\bar{P}$, is

$$\bar{P} = \frac{1}{(\omega_2 - \omega_1)} \int_{\omega_1}^{\omega_2} P(\omega)\, d\omega. \tag{1}$$

For discrete spectra, $\bar{P}$ is determined by the trapezoidal rule for numerical integration, which is accurate enough for this purpose.

The results of our Q measurements made by using individual gravimeter recordings are listed in Table 1. One notable disagreement with previously published determinations is for the mode ${}_0S_0$. Slichter (1967b) reported values of 14 960 and 11 010 (from gravimeters #4 and #7 respectively) for the recordings of the Alaskan earthquake. Extreme values such

Table 1. Values of Q and periods (T) obtained from gravimeter recordings. 'P_0' indicates the use of the power at the eigenfrequency to measure Q. 'Int.' indicates the use of the power integrated across the multiplet (equation (1)).

Mode	T	Q	Q^{-1} ($\times 10^3$)	σ/Q^{-1} ($\times 10^3$)	SD (%)	Record	Method
${}_0S_9$	634.41	326	3.07	0.163	5.3	Solomon	Int.
${}_0S_{10}$	580.69	286	3.50	0.108	3.1	Solomon	Int.
${}_0S_{12}$	502.65	335	2.98	0.239	8.0	Solomon	P_0
${}_0S_{13}$	473.72	305	3.28	0.126	3.8	Solomon	P_0
${}_0S_{14}$	447.93	298	3.36	0.349	10.4	Solomon	P_0
${}_0S_{16}$	407.38	259	3.86	0.224	5.8	Solomon	P_0
${}_0S_{17}$	389.74	316	3.17	0.210	6.6	Solomon	P_0
${}_0S_{19}$	360.48	251	3.99	0.191	4.8	Solomon	P_0
${}_0S_{24}$	306.08	149	6.70	0.877	13.1	Solomon	P_0
${}_0S_2$	3234.12	589	1.70	0.166	9.8	Alaska #7	P_0
${}_0S_3$	2134.72	460	2.18	0.188	8.6	Alaska #4	Int.
${}_0S_4$	1546.88	411	2.44	0.238	9.8	Alaska #4	Int.
${}_0S_5$	1190.84	352	2.84	0.913	32.1	Alaska #4	Int.
${}_0S_6$	962.82	343	2.92	1.012	34.7	Alaska #4	Int.
${}_0S_7$	812.09	373	2.68	0.343	12.8	Alaska #4	Int.
${}_0S_8$	708.24	357	2.80	0.371	13.3	Alaska #4	P_0
${}_0S_9$	634.22	284	3.52	0.196	5.6	Alaska #4	Int.
${}_0S_{10}$	580.48	329	3.04	0.199	6.5	Alaska #4	P_0
${}_0S_0$	1227.65	4229	0.24	0.013	5.3	Alaska #4	P_0
${}_0S_0$	1227.65	3996	0.25	0.028	11.2	Alaska #7	P_0
${}_1S_0$	613.25	1970	0.51	0.095	18.6	Alaska #4	P_0
${}_1S_7$	604.39	484	2.07	0.364	17.6	Alaska #4	Int.
${}_2S_4$	724.42	350	2.86	0.076	2.7	Alaska #4	Int.
${}_3S_1$	1057.89	1020	0.98	0.196	20.0	Alaska #4	Int.
${}_2S_0$	399.02	1170	0.85	0.045	5.3	Colombia	Int.
${}_2S_0$	399.02	1059	0.94	0.141	15.0	Colombia	P_0
${}_3S_0$*	305.55	874	1.14	0.050	4.4	Colombia	P_0
${}_4S_0$	243.58	989	1.01	0.056	5.5	Colombia	P_0
${}_5S_0$	204.56	824	1.21	0.204	16.9	Colombia	P_0
${}_6S_0$	174.16	933	1.07	0.086	8.0	Colombia	P_0
${}_3S_1$	1059.41	1020	0.98	0.019	1.9	Colombia	Int.
${}_4S_3$	489.12	560	1.79	0.431	24.1	Colombia	P_0
${}_5S_4$†	420.46	331	3.02	0.373	12.4	Colombia	P_0
${}_5S_5$‡	369.82	368	2.72	0.272	10.0	Colombia	P_0
${}_5S_6$§	331.88	341	2.93	0.310	10.6	Colombia	P_0
${}_8S_1$¶	348.57	704	1.42	0.167	11.8	Colombia	P_0
${}_{10}S_2$	247.81	870	1.15	0.126	11.0	Colombia	P_0
${}_{11}S_1$	271.37	508	1.97	0.044	2.2	Colombia	P_0
${}_{13}S_1$**	222.78	871	1.15	0.157	13.7	Colombia	P_0
${}_{13}S_2$	206.65	1125	0.89	0.009	1.0	Colombia	P_0

* Identified by Dratler *et al.* as '${}_4S_7$'
† Identified by Dratler *et al.* as '${}_4S_4$'
‡ Identified by Dratler *et al.* as '${}_4S_5$'
§ Identified by Dratler *et al.* as '${}_4S_6$'
¶ Identified by Dratler *et al.* as '${}_6S_1$'
** Identified by Dratler *et al.* as '${}_{10}S_1$'

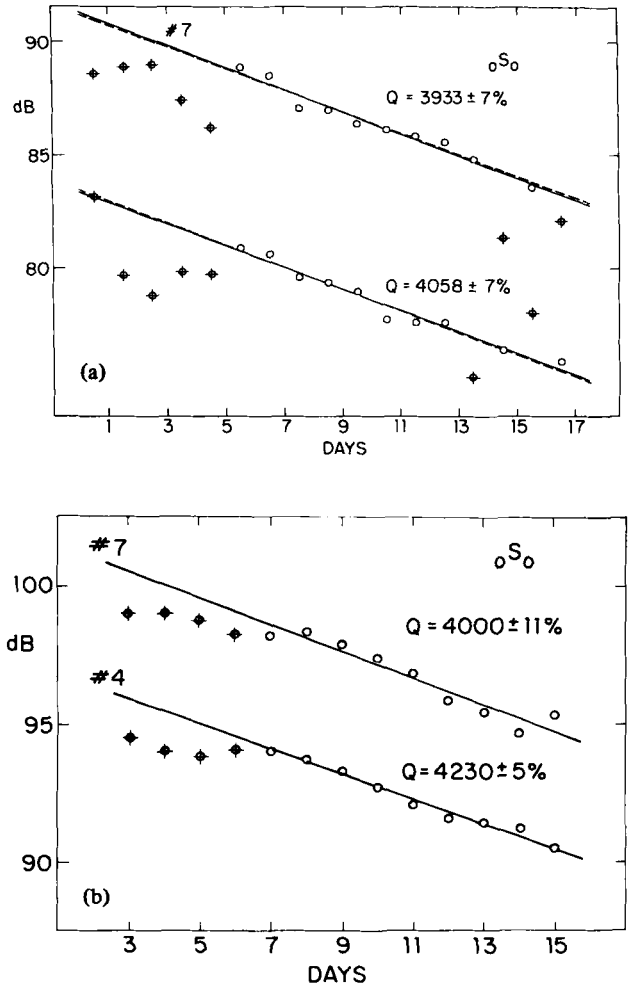

Figure 1. The attenuation of ${}_0S_0$ observed on gravimeters #4 and #7 in (a) one-day and (b) six-day windows. The points marked with crosses were not used in the regression fits shown. In (a) the dashed lines at the fit made to the data of both instruments simultaneously. Assuming the slope to be the same for both instruments, $Q = 4000 \pm 5$ per cent.

as 25 000 reported by Slichter *et al.* (1966) or 900 reported by Smith (1961) are definitely not consistent with the Alaskan recordings. Ness *et al.* (1961) concluded from the Chilean earthquake that Q for ${}_0S_0$ should be on the order of 7500. Indeed, a value of about 7000 is most consistent with nearly all reasonable Q_μ-only models, but we feel that there is good indication from the Alaska data that the proper value may be as low as 4000.

Fig. 1(a) shows the relative power of ${}_0S_0$ in one-day, non-overlapping windows. On both gravimeters, the first five days of data are unreliable. This may be due to interference from the mode ${}_0S_5$ which has been well excited, but has a Q lower than that of ${}_0S_0$ by an order of magnitude. This interpretation is supported by the fact that the effect is similar for both gravimeters, while their random noise shows no significant correlation. Fig. 1(a) also shows least-squares fits to the data from each gravimeter, taken separately, and a line fit to the data from both gravimeters. The latter is a three-parameter fit to 20 independent data points, assuming that the slope of the two lines must be the same while the intercepts are different.

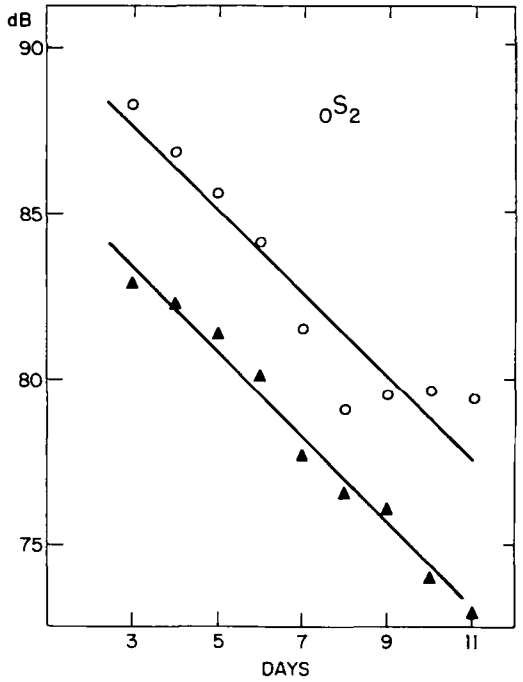

Figure 2. The attenuation of ${}_0S_2^{-1}$ (T = 3287.76 s) is shown by the open circles. Q is 581 ± 15 per cent. The solid triangles are $\bar{P}$ values from integrating across the entire multiplet (from T_1 = 3304.34 to T_2 = 3130.70). The line fit gives Q = 556 ± 5 per cent.

This three-parameter fit to the data from both gravimeters gives Q for ${}_0S_0$ of 4000 ± 5 per cent.

Fig. 1(b) shows the gravimeter data for ${}_0S_0$ as viewed through six-day windows. Since these windows overlap, the individual points shown are not independent and the statistics for the standard deviation of these Q measurements are not strictly valid. The use of longer, and overlapping, windows tends to smooth out the variation of power versus time. However, the results shown in Fig. 1(a) and (b) are consistent with one another.* For use in our inversion studies, we have adopted the value 4230 ± 5 per cent (shown in Fig. 1(b)) for Q of ${}_0S_0$.

Our observations for other modes fall within the wide range of previously published values, but they show considerable internal consistency and therefore appear to be reliable. Fig. 2 shows the attenuation of ${}_0S_0$. Since the $m = -1$ and $m = +1$ lines are resolvable, the Q measurements are not biased by splitting. Observations for ${}_1S_0$ and ${}_1S_7$ have not been previously published. The observed value of 484 for the Stoneley branch mode ${}_1S_7$ is not consistent with an extensive low Q zone at the base of the mantle.

3.2 STACKING

The technique of phase equalization or 'stacking' allows the recordings from many stations to be used simultaneously. When the earthquake source mechanism is known, all of the recordings made at different locations on the globe may be equalized in phase for a particu-

* For gravimeter #4, using all of the data points beyond the first six days gives 4200 ± 12 per cent for one-day windows, and 4230 ± 5 per cent for six-day windows. Using *all* of the data points for #4 gives 5183 ± 16 per cent for one-day windows, and 5663 ± 9 per cent for the six-day windows.

lar mode and then summed to enhance that mode. Phase equalization is accomplished by multiplying each recorded amplitude spectrum by the theoretical amplitude spectrum calculated for the desired mode at the appropriate location. Gilbert & Dziewonski (1975) present the theoretical basis for stacking, which rests on the fact that spherical harmonic functions are orthonormal over the unit sphere.

The spectral stack v_j (for the jth mode) is formed by multiplying each observed spectrum u_p by the theoretical spectrum of the jth mode at that station, before summing over a global array of stations:

$$v_j(\omega) = \sum_p a_{pj}(\omega) u_p(\omega) \tag{2}$$

the bar indicates complex conjugate, and the 'station' index p actually refers to each particular seismogram or component (i.e. N–S or E–W) used. The theoretical amplitudes $a_{pj}(\omega)$ may be calculated from a given earth model and source mechanism. We also include in a_{pj} a correction for the finite time duration of each seismogram. This correction is calculated according to equation (2.3.13) of Gilbert & Dziewonski (1975) and requires knowledge of theoretical values of the eigenfrequency (ω_j) and Q_j for the mode being stacked. We used Q_j calculated from model GDQ (Table 4).

Since the observed spectra u_p can be written as a superposition of normal modes, i.e. since

$$u_p(\omega) = \sum_k a_{pk} C_k(\omega), \tag{3}$$

and because of the orthogonality of spherical harmonics, v_j can be written as:

$$v_j(\omega) = \sum_k A_{jk}(\omega) C_k(\omega). \tag{4}$$

$C_k(\omega)$ is a 'resonance curve':

$$C_k(\omega) = \tfrac{1}{2}\left(\frac{\alpha_k + i(\omega_k - \omega)}{\alpha_k^2 + (\omega_k - \omega)^2} + \frac{\alpha_k - i(\omega_k + \omega)}{\alpha_k^2 + (\omega_k + \omega)^2}\right) \tag{5}$$

with its central peak being at the eigenfrequency, ω_k, and its shape or 'half-width' determined by Q_k, where $\alpha_k = \omega_k/2Q_k$. For positive frequencies the second term is negligible.

As Gilbert & Dziewonski show, the sum v_j in equation (4) contains only overtones of the desired jth mode, due to orthogonality. Since overtones are almost always well separated in frequency, stacking serves to isolate individual multiplets. Thus, from a spectral stack, we can measure both the eigenfrequency (ω_j) and the attenuation (α_j). The improvement in the signal to noise ratio provided by stacking allowed Gilbert & Dziewonski to identify eigenperiods for over 800 modes. In the present work, we measured Q for a relatively large number of modes (many of which cannot be observed in individual recordings). This is done simply by fitting a 'resonance curve' to each stack.

Since the stacks are assumed to approximate the shape of the resonance functions C_k, then

$$|v_k(\omega)| \simeq A_0 [\alpha_k^2 + (\omega_k - \omega)^2]^{-1/2}. \tag{6}$$

Obviously the problem of determination of α_k and ω_k from $|v_k(\omega)|$ is non-linear and starting values for A_0, ω_k and α_k are required. Equation (6) is perturbed with respect to A_0, α_k and ω_k:

$$\delta|v_k(\omega)| = [\alpha_k^2 + (\omega_k - \omega)^2]^{-1/2}\left(\delta A_0 - \frac{\alpha_k \delta\alpha_k + (\omega_k - \omega)\delta\omega_k}{\alpha_k^2 + (\omega_k - \omega)^2} A_0\right). \tag{7}$$

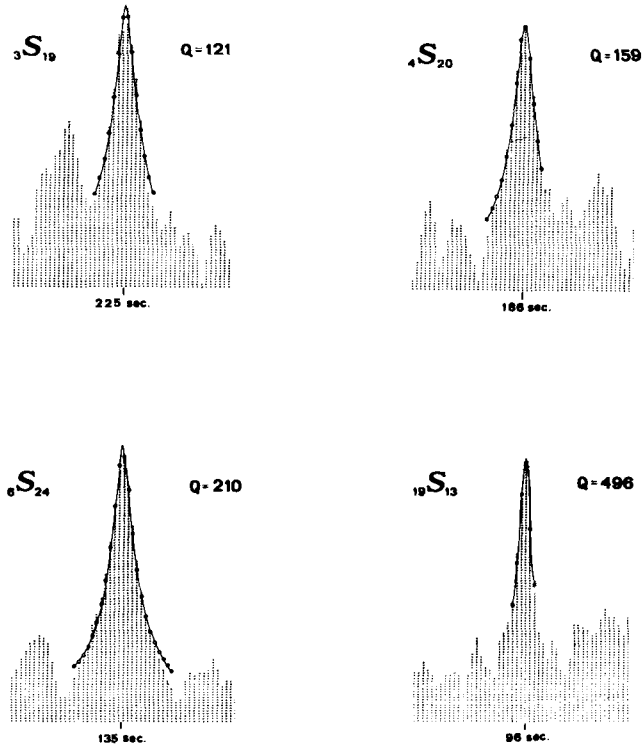

Figure 3. Examples of spectral stacks for spheroidal overtones. Resonance curves fitted to the stacks and measured Q values are shown. Each line in the stack is separated by 7.6×10^{-6} Hz.

Given values of $|v_k(\omega)|$ at a number of discrete frequencies ω, we solve for δA_0, $\delta\omega_k$ and $\delta\alpha_k$. Since we had reasonable starting values for ω_k and Q_k, this least-squares curve-fitting converges after several iterations. This gives a very stable estimate of α_k when enough points are used. Fig. 3 shows examples of stacks and the resonance curves which were fitted. The points to be fitted were chosen by inspecting the stacks. We used at least five points, always including the central peak, but avoiding obvious spikes of noise. In most cases we used 8 to 10 points, and for some stacks up to 25 points. If fits using different sets of points were not consistent, the mode was discarded as being contaminated by interference or noise.

Thus, starting with stacks for 812 modes (listed by Gilbert & Dziewonski 1975), we could obtain reasonable fits of a resonance curve for about 500 of these modes. However, only 197 of these modes had stacks of high enough quality that the fitted Q values could be considered reliable.

This method of Q measurement, just like any other, depends upon several assumptions. We assume that the network of stations provides good global coverage. However, the WWSSN stations are confined to land. Other departures from the ideal case include the finite time duration of the seismograms, the limited dynamic range of the recording system, random noise, and any inadequacies in the models used for earth structure and earthquake source mechanism. Numerical experiments have shown us that we have adequately corrected for the truncation of the seismograms. But the most important problem may be the splitting of multiplets caused by ellipticity, rotation and lateral heterogeneity of the Earth. In almost all cases, splitting causes an apparent broadening of a spectral peak. Thus, a Q measurement made from a stack will represent a lower bound on the Q of that multiplet. When more is

Table 2. Values of Q and periods obtained by stacking.

Mode	Q	T	Mode	Q	T
${}_0T_{13}$	118	506.10	${}_0S_{18}$	173	374.13
${}_0T_{22}$	114	333.42	${}_0S_{19}$	168	360.20
${}_0T_{23}$	123	321.80	${}_0S_{20}$	210	347.64
${}_0T_{30}$	111	257.77	${}_0S_{21}$	222	335.96
${}_0T_{32}$	133	244.15	${}_0S_{22}$	200	325.23
${}_0T_{36}$	131	220.46	${}_0S_{23}$	198	315.34
${}_1T_{7}$	238	475.19	${}_0S_{24}$	197	306.23
${}_1T_{9}$	178	407.65	${}_0S_{25}$	200	297.72
${}_1T_{11}$	176	359.09	${}_0S_{26}$	165	289.65
${}_1T_{12}$	195	339.50	${}_0S_{27}$	186	282.21
${}_1T_{14}$	151	307.06	${}_0S_{28}$	174	275.20
${}_1T_{19}$	151	249.80	${}_0S_{29}$	164	268.43
${}_1T_{22}$	172	225.30	${}_0S_{30}$	168	262.19
${}_1T_{24}$	139	211.85	${}_0S_{31}$	150	256.05
${}_1T_{26}$	202	200.41	${}_0S_{32}$	150	250.29
${}_1T_{28}$	155	190.05	${}_0S_{33}$	161	244.98
${}_1T_{29}$	186	184.96	${}_0S_{34}$	155	239.70
${}_1T_{30}$	165	180.90	${}_0S_{35}$	155	234.70
${}_1T_{34}$	155	165.45	${}_0S_{36}$	144	229.96
${}_1T_{35}$	173	162.34	${}_0S_{37}$	140	225.24
${}_1T_{36}$	147	159.05	${}_0S_{38}$	148	220.72
${}_1T_{37}$	180	156.08	${}_0S_{39}$	144	216.44
${}_1T_{38}$	169	152.89	${}_0S_{40}$	149	212.49
${}_1T_{39}$	164	150.24	${}_0S_{41}$	129	208.48
${}_1T_{44}$	157	138.12	${}_0S_{42}$	129	204.59
${}_1T_{50}$	166	126.01	${}_0S_{43}$	137	200.95
${}_1T_{60}$	153	110.58	${}_0S_{44}$	128	197.56
${}_2T_{28}$	139	158.37	${}_0S_{45}$	140	193.85
${}_2T_{29}$	175	154.66	${}_0S_{46}$	131	190.46
${}_2T_{34}$	169	138.61	${}_0S_{48}$	117	184.22
${}_2T_{36}$	183	133.12	${}_0S_{49}$	124	181.25
${}_2T_{37}$	172	130.55	${}_0S_{50}$	113	178.32
${}_2T_{52}$	162	102.58	${}_0S_{52}$	121	172.56
${}_3T_{11}$	150	240.41	${}_0S_{55}$	93	165.02
${}_3T_{19}$	173	178.14	${}_0S_{56}$	113	162.72
${}_3T_{20}$	207	173.01	${}_1S_{16}$	111	299.05
${}_3T_{23}$	128	158.69	${}_1S_{17}$	125	286.19
${}_3T_{24}$	174	154.43	${}_1S_{19}$	139	263.14
${}_3T_{25}$	176	150.60	${}_1S_{22}$	153	236.22
${}_3T_{26}$	264	147.10	${}_1S_{59}$	158	110.90
${}_3T_{27}$	296	143.72	${}_2S_{8}$	84	488.72
${}_3T_{29}$	362	137.24	${}_2S_{9}$	101	448.09
${}_3T_{30}$	215	134.13	${}_2S_{10}$	102	415.68
${}_3T_{53}$	236	91.23	${}_2S_{13}$	111	345.22
${}_4T_{11}$	208	199.55	${}_2S_{26}$	158	179.26
${}_4T_{17}$	204	169.63	${}_2S_{27}$	133	173.95
${}_4T_{20}$	144	155.85	${}_2S_{29}$	130	164.49
${}_4T_{23}$	189	143.68	${}_2S_{30}$	150	160.43
${}_5T_{9}$	243	174.26	${}_2S_{31}$	143	156.46
${}_5T_{10}$	157	171.95	${}_2S_{39}$	179	131.02
${}_0S_{13}$	276	473.27	${}_2S_{40}$	216	128.60
${}_0S_{14}$	247	448.26	${}_2S_{57}$	174	98.13
${}_0S_{15}$	227	426.33	${}_2S_{60}$	151	94.03
${}_0S_{16}$	253	406.92	${}_3S_{8}$	154	354.06
${}_0S_{17}$	195	389.56	${}_3S_{9}$	170	338.99

Table 2. *(Continued)*

Mode	Q	T	Mode	Q	T
${}_3S_{10}$	130	324.04	${}_6S_9$	292	252.69
${}_3S_{12}$	179	297.47	${}_6S_{17}$	147	165.99
${}_3S_{13}$	227	285.19	${}_6S_{18}$	208	160.39
${}_3S_{15}$	163	262.39	${}_6S_{20}$	203	150.18
${}_3S_{18}$	157	232.80	${}_6S_{21}$	194	145.73
${}_3S_{19}$	121	225.01	${}_6S_{23}$	186	138.07
${}_3S_{20}$	229	216.92	${}_6S_{24}$	210	134.89
${}_3S_{21}$	161	209.44	${}_6S_{25}$	171	131.84
${}_3S_{22}$	129	202.52	${}_6S_{31}$	171	116.49
${}_3S_{24}$	150	190.09	${}_6S_{32}$	182	114.16
${}_3S_{41}$	154	113.36	${}_6S_{36}$	152	106.18
${}_3S_{42}$	180	111.48	${}_6S_{47}$	276	89.15
${}_3S_{43}$	154	109.46	${}_7S_4$	277	293.32
${}_3S_{70}$	250	76.14	${}_7S_6$	223	252.69
${}_4S_9$	169	269.71	${}_7S_7$	238	236.30
${}_4S_{11}$	204	249.13	${}_7S_{16}$	251	154.47
${}_4S_{14}$	201	225.05	${}_7S_{20}$	222	141.17
${}_4S_{20}$	159	186.24	${}_7S_{21}$	205	138.01
${}_4S_{24}$	206	165.59	${}_7S_{22}$	206	135.03
${}_4S_{31}$	264	138.69	${}_7S_{46}$	311	85.16
${}_4S_{32}$	299	135.59	${}_7S_{57}$	339	73.75
${}_4S_{33}$	159	132.66	${}_8S_9$	483	192.06
${}_4S_{34}$	219	129.85	${}_8S_{15}$	321	158.55
${}_4S_{35}$	246	127.08	${}_9S_7$	235	204.96
${}_4S_{36}$	176	124.57	${}_9S_{11}$	320	169.98
${}_4S_{39}$	193	117.64	${}_9S_{12}$	348	161.60
${}_5S_7$	496	303.67	${}_9S_{13}$	302	154.25
${}_5S_8$	247	282.93	${}_{10}S_{14}$	255	142.07
${}_5S_{10}$	305	237.92	${}_{10}S_{15}$	347	138.77
${}_5S_{11}$	222	224.59	${}_{10}S_{25}$	271	101.80
${}_5S_{25}$	231	143.63	${}_{10}S_{28}$	399	95.65
${}_5S_{26}$	236	140.22	${}_{10}S_{42}$	264	78.03
${}_5S_{28}$	164	134.17	${}_{11}S_3$	368	223.97
${}_5S_{29}$	203	131.08	${}_{11}S_4$	652	209.68
${}_5S_{30}$	248	128.55	${}_{12}S_7$	300	170.69
${}_5S_{31}$	182	125.82	${}_{13}S_1$	1573	222.65
${}_5S_{36}$	204	114.75	${}_{13}S_{26}$	435	89.36
${}_5S_{37}$	171	112.70	${}_{15}S_{32}$	360	74.87
${}_5S_{38}$	223	110.65	${}_{16}S_{20}$	463	88.74
${}_5S_{39}$	179	108.72	${}_{17}S_{24}$	435	79.80
${}_5S_{40}$	178	106.86	${}_{18}S_{16}$	331	93.38
${}_5S_{41}$	195	105.06	${}_{19}S_{13}$	496	95.90
${}_5S_{42}$	169	103.43	${}_{20}S_{18}$	630	83.12
${}_5S_{44}$	216	100.21			

learned about the extent of lateral heterogeneity, it may be possible to take this effect into account. Thus it is difficult at present to estimate the magnitude of errors in these Q measurements. They can best be judged by comparison with results of other studies, and by their internal consistency (as indicated by inversion).

In Table 2 we list the values of Q for 197 modes, obtained by stacking with the correction for truncation. These modes were chosen on the basis of having the best stacks. They include 50 toroidal modes, 40 ${}_0S_l$ ($13 \leqslant l \leqslant 56$), and 107 spheroidal overtones. The

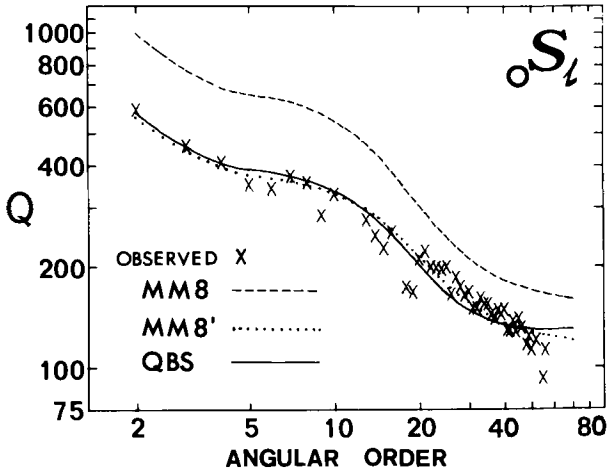

Figure 4. Observed values of Q for the fundamental spheroidal mode. The values predicted by three different Q models are shown.

Q values for the fundamental spheroidal modes, shown in Fig. 4, are in good agreement with observations of Rayleigh waves (e.g. Kanamori 1970). These values decrease smoothly with increasing l, as should be expected. However, the overtones have a much greater scatter in Q values for a given n and different values of l. This must be due to the effects of noise and scattering by lateral heterogeneities.

4 Inversion

4.1 THEORY

To obtain a model of the variation of attenuation with radius in the Earth, $Q^{-1}(r) \equiv q(r)$, which satisfies a set of measurements of Q^{-1} of normal modes, one must solve a linear inverse problem. In this paper we consider two approaches to finding solutions: parameter-space inversion and data-space inversion. Each approach has distinct advantages; we will use both and compare the results.

The parameter-space inversion has been widely used in geophysics (*cf.* Wiggins 1972). The first step in this case is to parameterize the model space – i.e. decide how the model function will be represented in terms of a finite number, m, of parameters. The inversion will then give specific values for the parameters representing a model that satisfies the data.

The simplest parameterization of q variation, for example, would be to assume that $q(r)$ is constant within each of m spherical shells. A simple linear relationship exists between q_i (the parameter value of q in the ith shell) and Q_j^{-1}, the observed value of Q^{-1} for the jth normal mode:

$$Q_j^{-1} = \sum_{i=1}^{m} G_{ij} q_i \tag{8}$$

where the G_{ij} are partial derivatives of Q_j^{-1} with respect to q_i.

If we have observed Q_j^{-1} for n different modes, then equation (15) represents a system of n linear equations with m unknowns. When $n > m$, we can find a particular solution known as the least-squares solution. If we know the uncertainty, or the standard deviation of each observation, then the weighted least-squares solution is appropriate.

The data-space inversion has been extensively discussed by Backus & Gilbert (1967, 1968, 1970). They represent physical parameters as piecewise continuous functions of radius. The relationship of the observed quantity to the model is given by an inner product between the model and a Fréchet kernel. For example,

$$Q_j^{-1} = \int_0^1 [\mu(r)\tilde{M}_j(r)q_\mu(r) + K(r)\tilde{K}_j(r)q_K(r)]\, r^2\, dr. \tag{9}$$

The functions $\tilde{M}_j(r)$ and $\tilde{K}_j(r)$ are defined in Backus & Gilbert (1967; equation 30, 31) and $\mu(r)$ and $K(r)$ are the shear and bulk moduli, respectively. This equation (*cf.* Backus & Gilbert 1968) is analogous to the expression for Q^{-1} of Rayleigh waves given by Anderson & Archambeau (1964). However, in addition to its simplicity, this expression provides a greater physical insight, as the quantities $\mu\tilde{M}_j$ and $K\tilde{K}_j$ are the densities of the shear and compressional energies, respectively.

Of course, it is not necessary to use the continuous function representation in order to perform inversion in the data space -- this is just the most general notation.

Now, there are an infinite number of model functions $q(r)$ which will satisfy a given set of observations, but we would like to find some particular solution which will be meaningful. One approach is to extract, from the space of all models which satisfy the data, the one model which differs minimally from some starting model. This minimization is constrained by the observations; that is, find

$$\min \int_0^1 [\delta m(r)]^2 r^2 dr \tag{10}$$

subject to the constraints

$$\delta d_j = \int_0^1 \delta m(r)\mathscr{S}_j(r)r^2 dr, \tag{11}$$

where δm is the difference between the final model and the starting model, and δd_j are the differences between the observed value for each datum and the value predicted by the starting model. The solution to this minimization with constraints is found by introducing the Lagrange multipliers α_j, as used by Backus & Gilbert (1967).

We note that equation (11) is correct to first order in δm and is exact for linear inverse problems. Thus, it is not necessary, in order to satisfy the data, to use a 'starting model'; or the 'starting model' could be $q(r) = 0$ everywhere. However, the resolving power of a finite data set is always limited, and it can be instructive to investigate whether certain *a priori* assumed features of the models are consistent with the data set.

For our data-space inversions, we have made the more realistic assumption that the data contain errors. We relax the constraints (11) and do not require that the data be satisfied exactly, but that each datum be satisfied within a standard error:

$$\delta d_j - \sigma_j \leqslant \int_0^1 \delta m(r)\mathscr{S}_j(r)r^2 dr \leqslant \delta d_j + \sigma_j. \tag{12}$$

We apply the technique called 'ranking and winnowing' of Gilbert (1971). This is a method of finding the Lagrange multipliers by transformation of the data space and then considering each datum in the order of its significance, eventually rejecting data with large errors and associated small eigenvalues. The inequality constraints can be satisfied very simply by choosing the Lagrange multipliers in the proper way. This is done by simultaneously

diagonalizing the inner product matrix

$$\mathcal{A}_{ij} = \int_0^1 \mathcal{S}_i \mathcal{S}_j r^2 dr$$

and the covariance matrix V_{ij}. The transformation $\mathbf{T}$ such that $\mathbf{T}\mathcal{A}\mathbf{T}^T = \mathbf{I}$ and $\mathbf{TVT}^T = \mathbf{E}$, (where $\mathbf{I}$ is the identity matrix and $\mathbf{E}$ is diagonal), is easy to calculate and is given by Gilbert (1971). The transformed observed values and the transformed kernels are $\mathbf{T}\delta\mathbf{d}$ and $\mathbf{T}\mathcal{S}$, respectively. These are used in place of $\delta\mathbf{d}$ and $\mathcal{S}$ in order to find the Lagrange multipliers. Thus, the transformed kernels represent different linear combinations of the original kernels. Each transformed kernel is associated with an eigenvalue of the inner product matrix, and for the largest eigenvalues with a 'significant earth datum' (SED). Several transformed kernels for a set of 38 modes are shown in Fig. 8, which will be referred to later.

4.2 RESULTS

4.2.1 Data space inversion

In order to obtain the general model features that the data require, without a prejudicial choice of parameterization, we first performed inversion in the data space. (For any type of inversion, an elastic earth model, $\rho(r), \mu(r), K(r)$, must first be assumed in order to calculate the kernels $\tilde{M}$ and $\tilde{K}$. We used model PEM-A of Dziewonski, Hales & Lapwood (1975).)

The set of 38 modes selected for data-space inversion is given in Table 3. There are 21 ${}_0S_l$ modes from ${}_0S_2$ to ${}_0S_{65}$, seven radial modes from ${}_0S_0$ to ${}_6S_0$, six high-Q spheroidal overtones, three toroidal modes and one Stonely branch mode $-{}_1S_7$. For 29 of these 38 modes, Q was measured from the gravimeter records of one of the three large earthquakes. The other nine modes in this selected data set are from the stacking results. They are the three toroidal modes and ${}_0S_{20}$, ${}_0S_{30}$, ${}_0S_{40}$, ${}_0S_{50}$, ${}_0S_{60}$ and ${}_0S_{65}$.

The method of ranking and winnowing makes use of the standard errors σ_j of the data for inequality constraints in inversion. The final results will depend upon the relative precision of the different measurements.

For the modes observed on individual gravimeter recordings, the initial error estimates were obtained directly from the least-squares fit which determined Q. However, these estimates may not accurately reflect the true uncertainty in the value of Q for these modes. Rather, these estimates may represent lower bounds on the true uncertainty. This is because the quality of the line fit obtained from a single record does not fully reflect the true uncertainty and repeatability of a Q measurement for a given mode. The line fit which gives the measured value of Q may have a very small variance, yet the uncertainty in the Q value for this particular mode may be large.

Of the 29 modes measured by single recording, we found it reasonable to increase the error estimates for 13 of these. We subjectively re-estimated standard errors for those modes which might be subject to interference from other modes. The final result was that for the set of 38 modes all had SD greater than 5 per cent (SD = $(\sigma_j/Q_j) \times 100$ per cent). For most modes SD was 10 per cent or less, and for four modes, SD was 20 per cent or greater.

For the Q observations made by stacking, the errors were subjectively estimated. Note that the shorter period modes, while affected less by ellipticity splitting, would be biased more by splitting due to lateral heterogeneities. In fact, the modes ${}_0S_{60}$ and ${}_0S_{65}$ had poorer stacks and were not among the set of 197 'best' observations listed in Table 2.

In what follows, we describe the goodness of fit of different models in terms of their

Table 3. Q observations, and Q values predicted by ten different models, for a representative set of 38 modes.

Mode	Q	SD (%)	QMU	GDQ	MM8	MM8′	L3L	L3L′	$Q\overline{200}$	$Q\overline{200}'$	QBS	QKB
${}_0T_{22}$	114	9.0	119	124	150	114	129	122	200	123	128	124
${}_0T_{30}$	111	9.0	114	118	139	106	125	118	200	118	124	118
${}_1T_{36}$	147	9.0	140	147	198	144	150	141	200	143	146	147
${}_0S_0$	4230	5.3	7034	7520	10068	6934	7678	7259	7554	6906	4271	4315
${}_1S_0$	1970	18.8	2147	2442	4474	2249	1943	1957	1270	2012	2078	1656
${}_2S_0$	1170	15.0	1607	1780	2965	1705	1776	1704	1175	1558	1364	1205
${}_3S_0$	874	15.0	1361	1478	2329	1462	1318	1268	1205	1308	1100	1003
${}_4S_0$	989	10.0	1156	1241	1901	1241	1214	1167	1171	1156	918	898
${}_5S_0$	824	16.8	1119	1198	1811	1198	1124	1083	1177	1149	896	906
${}_6S_0$	933	15.0	1258	1357	2051	1321	1264	1222	1206	1249	1058	1043
${}_0S_2$	589	9.8	540	602	997	559	497	493	370	510	576	577
${}_0S_3$	460	8.6	435	482	771	446	407	402	314	415	455	458
${}_0S_4$	411	9.8	388	430	684	397	372	367	281	373	407	409
${}_0S_5$	352	32.1	371	411	655	378	363	359	266	357	391	391
${}_0S_6$	343	34.7	363	403	641	369	363	358	258	351	382	381
${}_0S_7$	373	12.8	357	396	625	361	365	359	254	346	373	373
${}_0S_8$	357	13.2	349	388	602	351	368	360	252	340	362	361
${}_0S_9$	284	10.0	341	377	575	341	369	358	251	333	349	349
${}_0S_{10}$	329	6.5	331	364	547	330	365	352	251	323	335	335
${}_0S_{12}$	335	8.0	306	335	492	308	344	327	251	299	307	308
${}_0S_{13}$	305	5.0	292	319	465	296	328	311	251	286	292	293
${}_0S_{14}$	298	10.4	278	302	437	283	311	294	250	273	277	279
${}_0S_{16}$	259	5.8	250	269	386	258	277	261	249	248	248	250
${}_0S_{19}$	251	10.0	213	227	322	224	234	220	247	216	211	214
${}_0S_{20}$	210	9.0	203	215	305	214	222	209	246	207	201	204
${}_0S_{24}$	149	13.1	173	181	253	183	187	176	242	179	171	174
${}_0S_{30}$	168	9.0	148	155	211	156	160	150	237	155	148	150
${}_0S_{40}$	149	9.0	132	138	182	136	143	135	231	135	134	134
${}_0S_{50}$	113	9.0	127	132	170	127	138	130	227	127	130	129
${}_0S_{60}$	110	9.0	125	130	164	123	137	128	225	124	129	127
${}_0S_{65}$	137	9.0	125	129	162	121	136	128	225	123	129	127
${}_1S_7$	484	17.6	406	459	814	423	424	419	250	383	448	446
${}_2S_4$	350	5.0	375	407	603	383	374	365	332	369	378	384
${}_3S_1$	1020	20.0	856	942	1052	895	842	821	664	828	846	874
${}_5S_5$	368	15.0	481	522	818	516	499	480	436	476	472	495
${}_5S_6$	341	15.0	487	529	836	522	516	496	433	485	464	492
${}_8S_1$	704	15.0	1074	1163	1185	1149	1142	1091	983	1072	935	970
${}_{13}S_2$	1125	20.0	1075	1154	1756	1149	1115	1074	1099	1101	874	924
		$\bar{\chi}$	1.70	1.92	4.19	1.72	1.94	1.77	3.56	1.70	1.05	1.02
		rms	0.17	0.19	0.42	0.18	0.18	0.17	0.37	0.17	0.13	0.13

relative rms error and the parameter $\bar{\chi}$, where

$$\text{rms} = \left[\frac{1}{n}\sum_{j=1}^{n}\left(\frac{1/Q_j - 1/Q_j}{1/Q_j}\right)^2\right]^{1/2}$$

$$\bar{\chi} = \left[\frac{1}{n}\sum_{j=1}^{n}\left(\frac{1/Q_j - 1/Q_j}{\sigma_j}\right)^2\right]^{1/2} \qquad (13)$$

For the weighted (by relative errors) inversions, including 'ranking and winnowing', the appropriate measure of goodness of fit is $\bar{\chi}$.

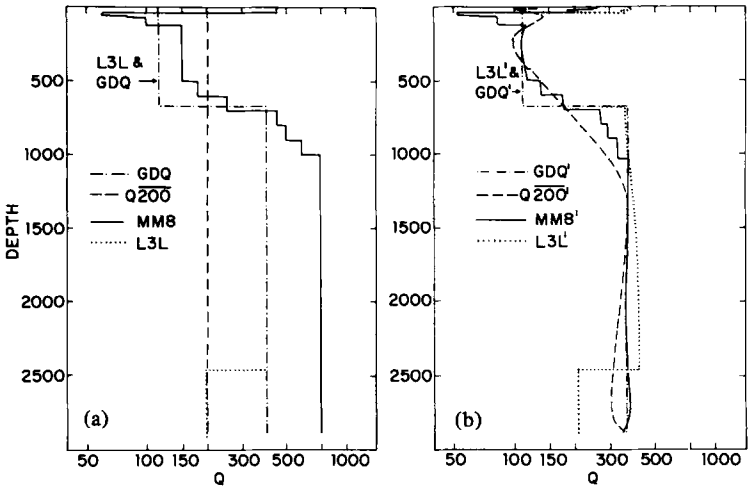

Figure 5. (a) Four representative 'starting models' of Q_μ in the mantle. (b) The corresponding models obtained by data-space inversion using three eigenvalues. These models represent the smallest perturbation to the 'starting model' subject to the constraints of the observed values of Q for 38 modes.

Figs 5–8 summarize the results of data-space inversion for Q_μ in the mantle. These calculations have produced a group of models which satisfy the data as well as possible given the assumptions that $Q_K = \infty$ everywhere, and that $Q_\mu = \infty$ in the core. They indicate the variation of Q_μ unbiased to the first order by an arbitrary choice of parameters (i.e. layer locations). Fig. 5(a) shows four different starting models. These models do not satisfy the observations very well. For example, model $Q\overline{200}$ has a constant Q_μ of 200 throughout the mantle. This is roughly the correct average mantle Q, but this model has an incorrect radial variation of Q_μ. Model MM8 of Anderson, Ben-Menahem & Archambeau (1965) has a more reasonable form of radial Q variation, but Q_μ is too high in the lower mantle.

From the starting models shown in Fig. 5(a), the 'ranking and winnowing' data-space inversion using three eigenvalues produced the corresponding Q models shown in Fig. 5(b). Model $Q\overline{200}'$ (derived from $Q\overline{200}$) has a smooth variation of Q_μ which reaches a maximum value of 370 in the lower mantle. As shown by Table 3, all of these models ($Q\overline{200}'$, MM8', etc.) satisfy the observations better than the starting models. All of these models have $Q_\mu \simeq 350$ in the lower mantle. Another important result is that $\bar{Q}_{ScS}$, the value of Q that would be observed for vertical ScS, ranges between 210 and 217 for all of the final models.

Starting models with low-Q zones in the lower 350 km preserve this feature through ranking and winnowing inversion. The resulting models (e.g. L3L') can satisfy the data nearly as well as those models which are constant in the entire lower mantle – provided that the average Q in the low-Q layer is not less than 200. We conclude that the presence of such a low-Q layer cannot be resolved with this data set.

The resolution of our data set and the stability of models can be considered informally in terms of eigenvalues used in the data-space inversion. In ranking and winnowing, we find the eigenvalues of the transformed inner product matrix in order of decreasing size. The first (largest) eigenvalue is associated with the most significant datum, and so on. As we use the smaller eigenvalues, and hence the less significant combinations of the data, the fit will improve only slightly. Eventually, the inverse becomes unstable, and we get models with negative Q. Fig. 6 shows a progression of different Q^{-1} models, all obtained from starting model MM8, but using different numbers of eigenvalues. When five or six eigenvalues have been used, two minima in the variation of Q_μ^{-1} begin to develop in the lower mantle. As

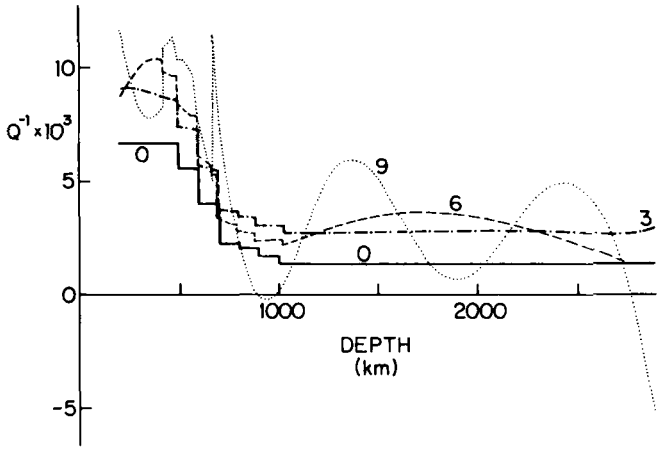

Figure 6. The development of model instability in data-space inversion. Starting model MM8 (0) and models derived from it using three, six and nine eigenvalues.

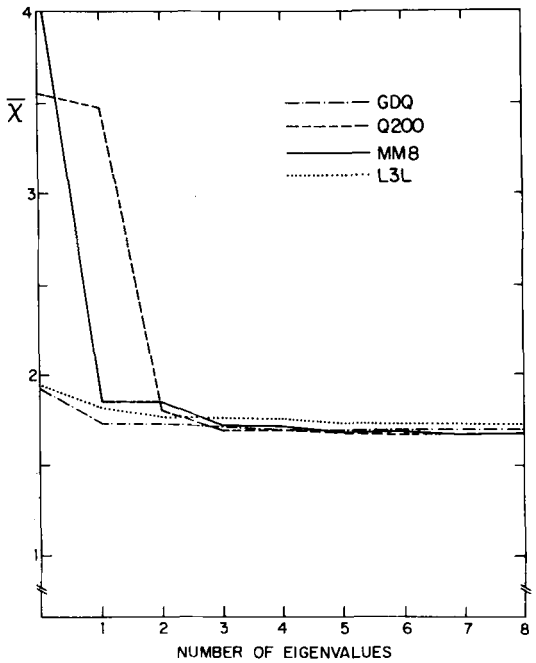

Figure 7. The progressive improvement in the fit of models to a set of 38 observations as more eigenvalues are used in the data space inversion. $\bar{\chi}$ is defined in the text (equation (13)).

additional eigenvalues are used, the fit does not improve much, but these minima become more pronounced. Finally, when nine eigenvalues have been used, Q_μ^{-1} becomes negative here. This type of behaviour occurs with all starting models. As Fig. 7 shows, the fit to the observations does not improve much after three or four eigenvalues have been used. Thus, features which appear in models when more than four eigenvalues are used are due only to instability in the inversion.

The resolution provided by each significant earth datum, or more properly, the form of the perturbation that each transformed kernel can make to any starting model, is shown by

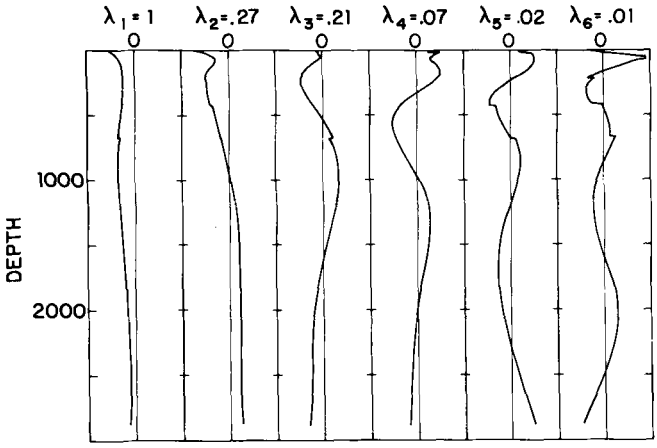

Figure 8. The first six transformed kernels ($T\mathscr{S}$) for a representative data set of 38 modes. Each kernel is plotted on a scale from -1 to $+1$, and is normalized by the corresponding eigenvalue. The ratio of each eigenvalue to the first (largest) eigenvalue is given.

Fig. 8. The first transformed kernel has the same sign throughout the mantle. Because of this, an inversion using only the first eigenvalue will produce a model which is a correction of the starting model to the proper average mantle Q. So, regardless of the starting model used, $\bar{Q}_{ScS}$ is roughly 210 after the first eigenvalue is used. The second transformed kernel changes sign once in the mantle, and allows resolution of differences in Q between the upper and lower mantle. Thus, the transformed kernels do indicate the rather limited resolution that is provided by our representative set of 38 modes. But even if we could greatly increase the number of Q observations, the number of SED would remain small unless the errors of the data could be significantly reduced.

We have shown that simple Q models can describe the data adequately. But if we consider the residuals for each of these models (see Table 3) we see that the radial modes are not fitted very well by any of the models for Q_μ in the mantle. The predicted values are higher than the observed values for all of the radial modes. These modes are dominated by compressional energy (*cf.* Dziewonski & Gilbert 1972, Table 7). Thus, by allowing finite bulk dissipation ($Q_K^{-1} > 0$) we could satisfy the observations of Q for radial modes and improve the overall fit. However, the data-space inversion that allows both Q_K and Q_μ to vary everywhere in the earth model is very unstable. This is because the radial modes, which are analogous to PKIKP body waves, cannot resolve the region in which bulk dissipation may occur. But our experiments indicate that the two most likely regions for bulk dissipation are the inner core and the upper mantle.

4.2.2 Parameter space inversion

The previous discussion has shown that our data set contains only very few significant earth data (SED). It is reasonable then to perform inversion in the parameter space using only a few parameters. We will divide the mantle into two shells, with the boundary at 670 km depth. In this section we will first describe the parameter-space inversion for Q_μ, then the inversion for both Q_μ and Q_K.

The two-shell Q_μ model with $Q_\mu = 108$ in the upper mantle, $Q_\mu = 346$ in the lower mantle, was obtained by parameter-space inversion of the set of 38 modes without consideration of their relative errors. The variance of the parameters is such that within one

Table 4. Parameter values of simple Q models. All models (except GDQ) were obtained by inversion of the 38 modes listed in Table 3. In the regions not specified, Q_μ and/or $Q_K = \infty$.

Parameter	GDQ	QMU	QML	QBS	QKB
Q_μ lithosphere (0–80 km)	115	111	200	200	115
Q_K upper mantle (80–670 km)	∞	∞	∞	433	742
Q_μ upper mantle (80–670 km)	115	111	102	110	115
Q_μ lower mantle (670–2885 km)	400	350	344	403	395
Q_K inner core (5154–6371 km)	∞	∞	∞	∞	1227
$\bar{\chi}$	1.92	1.70	1.67	1.05	1.02
rms	0.19	0.17	0.16	0.13	0.13
$\bar{Q}_{ScS}$	230	213	209	232	228

standard deviation of $1/Q$, Q_μ could be from 103 to 113 in the upper mantle, and from 326 to 368 in the lower mantle. $\bar{Q}_{ScS}$ for this model is 210. If the observations are weighted by their standard errors, the result is not much different: $Q_\mu = 111 \pm 4$ per cent, 350 ± 5 per cent ($\bar{\chi} = 1.70$, rms = 0.17). These simple two-shell models satisfy the data as well as the smoother and slightly more detailed models obtained by data-space inversion. The latter model (111, 350) is referred to as QMU in Tables 3 and 4.

When we consider only the data obtained by stacking (Table 2), the two-shell inversion gives a model with a lower value of Q_μ in the lower mantle. The model obtained by inverting 197 modes has $Q_\mu = 121 \pm 4$ per cent in the upper mantle and $Q_\mu = 264 \pm 6$ per cent in the lower mantle, $\bar{Q}_{ScS} = 195$, and rms = 0.23. The result when both data sets are combined is 117 ± 3 per cent, and 291 ± 4 per cent, $\bar{Q}_{ScS} = 201$ and rms = 0.22. Note that the representative set of 38 modes observed mainly on individual gravimeter recordings implies that Q is from 332 to 369 in the lower mantle. This shows that the observations from stacking are biased, as expected, towards lower Q because of splitting. However, these observations do provide a reasonable lower bound on Q_μ in the mantle, and give a consistent estimate of $\bar{Q}_{ScS}$. Thus we reaffirm our earlier conclusion that Q_μ in the lower mantle is less than had generally been thought (Sailor & Dziewonski 1976). This conclusion is also supported by recent observations of Q for multiple ScS. While some measurements of $\bar{Q}_{ScS}$ were as high as 600 (Kovach & Anderson 1964), Jordan & Sipkin (1977) report a value of 156. The attenuation of S waves predicted by our models is also consistent with the results of Brune (1977).

Since none of the Q_μ-only models can satisfy the radial modes, we next try two-shell inversions, allowing both Q_K and Q_μ to vary in each layer. In this case, instability develops so that Q_K is found to be $-20\,000$ in the lower mantle. Of course this indicates that Q_K^{-1} is essentially zero in the lower mantle, so we are justified henceforth to constrain it to be zero in that region.

The best-fitting model, designated as QKB in Tables 3 and 4, has $Q_K = 1227$ in the inner core and $Q_K = 742$ in the upper mantle. Q_μ is 115 in the upper mantle and 395 in the lower mantle. Another model, with Q_K finite in the upper mantle only, is: $Q_K = 448$; $Q_\mu = 117$, 410; $\bar{\chi} = 1.08$ and rms = 0.13. A model with finite Q_K in the inner core only is: $Q_K = 605$; $Q_\mu = 111, 368$; $\bar{\chi} = 1.12$, rms = 0.14.

Our best-fitting model for dissipation in the mantle is designated as QBS – for Q, bulk and shear. In the upper mantle, $Q_\mu = 110 \pm 4$ per cent and $Q_K = 433 \pm 13$ per cent. In the lower mantle (below 670 km), $Q_\mu = 403 \pm 6$ per cent and $Q_K = \infty$. There is a lithosphere 80 km thick in which Q_μ was constrained to be 200. See Table 4 for comparison of QBS with the corresponding Q_μ-only model, called QML.

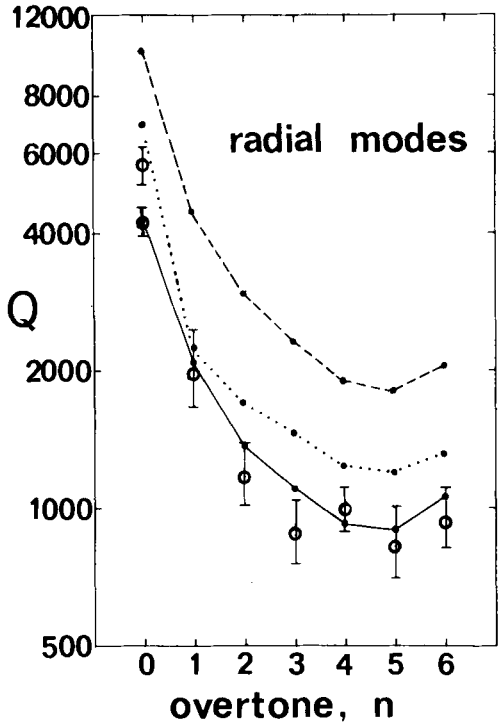

Figure 9. Observations of Q for radial modes and values predicted by three different Q models. Model QBS (solid line) has $Q_K = 433$ in the upper mantle and is the best fit to these modes. Model MM8 (dashed line) and model MM8′ (dotted line) predict Q values too high.

The fit of model QBS to the fundamental spheroidal and the radial modes is compared with that of other models in Figs 4 and 9. Fig. 4 shows that the fundamental spheroidal modes are not sensitive to bulk dissipation. Model MM8, which has $Q_\mu = 750$ in the lower mantle, does not satisfy these modes (rms = 32 per cent for 48 modes). But model MM8′ and model QBS both satisfy this subset of the data equally well (rms of 9 and 11 per cent, respectively). Fig. 9 shows that the radial modes provide the best discriminant among these models. For the seven radial modes, model MM8 had an rms of 56, MM8′ – 31 and QBS – 11 per cent.

So, we have shown that bulk dissipation may occur in the inner core or upper mantle. At present, we consider bulk dissipation in the upper mantle to be the more interesting hypothesis. Physical mechanisms do exist to explain this, such as motion of a phase-change boundary (Vaisnys 1968), or induced flow of partial melt (R. J. O'Connell 1977, private communication). Furthermore, this sort of Q distribution is not inconsistent with velocity dispersion due to anelasticity (Dziewonski 1977). Further observations of the radial modes, and modes which contain much compressional energy in the upper mantle, will be necessary to check this hypothesis.

5 Conclusions

Our observations and inversion of normal mode attenuation lead to three main conclusions:

(1) The average value of Q in the lower mantle is approximately 400, and $\bar{Q}_{ScS}$ is between 200 and 230.

(2) A large number of Q observations can be explained by rather simple two or three-shell models. The reason why more complicated models are not justified at the present time is that the data set considered here cannot resolve much detail, and the observations themselves contain fairly large uncertainties. Our opinion is that one should not use extremely detailed Q models when it can be shown that simple models satisfy the data just as well.

(3) Q_K is finite in the upper mantle and possibly in the inner core. This conclusion is subject to verification by additional observations of Q for radial and other 'high-Q' modes. We consider the upper mantle to be the more plausible possible site for bulk dissipation. Simultaneous inversion for Q_μ and Q_K has shown that the data can be satisfied quite well if Q_K is infinite in the inner core and lower mantle, but finite in the upper mantle. The exact value of Q_K in the upper mantle is not certain – we estimate the average value for the upper 670 km to be approximately 450, if $Q_K^{-1} = 0$ outside of this region.

We must emphasize that the models we have derived are only descriptive of the gross-earth attenuation in the period range from about 100 to 3000 s. There does not seem to be any indication of frequency dependence of Q in this period range (Sailor & Dziewonski 1976). However, the uncertainty of Q observations needs to be greatly reduced before this question can be settled. Our Q measurements are consistent with shear-wave attenuation studies down to periods as short as 20 s (Brune 1977; Jordan & Sipkin 1977). Body-wave studies at shorter periods give conflicting results and further investigation is necessary.

Acknowledgments

We thank Professor L. B. Slichter of the University of California, Los Angeles, for providing us with the digital recordings of the Alaskan earthquake. Professors F. Gilbert and T. H. Jordan and Dr R. P. Buland, all of the University of California, San Diego, were very helpful throughout this study, and gave us copies of the gravimeter recordings of the Colombia and Solomon Islands earthquakes.

R. V. Sailor has been supported by a Graduate Fellowship from the National Science Foundation. This research has been supported by grants EAR72-01344 and EAR76-14839 from the National Science Foundation.

References

Akopyan, S. Ts., Zharkov, V. N. & Lyubimov, V. M., 1975. The dynamic shear modulus in the interior of the Earth, *Doklady, Earth Sci. sec.*, **223**, 1–3.

Akopyan, S. Ts., Zharkov, V. N. & Lyubimov, V. M., 1976. Corrections to the eigenfrequencies of the Earth due to the dynamic shear modulus, *Phys. Solid Earth*, **12**, 625–630.

Alsop, L. E., Sutton, G. H. & Ewing, M., 1961. Measurement of Q for very long period free oscillations, *J. geophys. Res.*, **66**, 2911–2915.

Anderson, D. L. & Archambeau, C. B., 1964. The anelasticity of the Earth, *J. geophys. Res.*, **69**, 2071–2084.

Anderson, D. L., Ben-Menahem, A. & Archambeau, C. B., 1965. Attenuation of seismic energy in the upper mantle, *J. geophys. Res.*, **70**, 1441–1448.

Backus, G. & Gilbert, F., 1967. Numerical applications of a formalism for geophysical inverse problems, *Geophys. J. R. astr. Soc.*, **13**, 247–276.

Backus, G. & Gilbert, F., 1968. The resolving power of gross Earth data, *Geophys. J. R. astr. Soc.*, **16**, 169–205.

Backus, G. & Gilbert, F., 1970. Uniqueness in the inversion of inaccurate gross Earth data, *Phil. Trans. R. Soc. Lond. A*, **266**, 123–192.

Benioff, H., Press, F. & Smith, S., 1961. Excitation of the free oscillations of the Earth by earthquakes, *J. geophys. Res.*, **66**, 605.

Brune, J. N., 1977. Q of shear waves estimated from S–SS spectral ratios, *Geophys. Res. Lett.*, **4**, 179–181.

Buland, R. & Gilbert, F., 1978. Improved resolution of complex eigenfrequencies in analytically continued spectra, *in press.*

Deschamps, A., 1977. Inversion of the attenuation data of free oscillations of the Earth (fundamental and first higher modes), *Geophys. J. R. astr. Soc.*, **50**, 699–722.

Dratler, J., Farrell, W. E., Block, B. & Gilbert, F., 1971. High-Q overtone modes of the Earth, *Geophys. J. R. astr. Soc.*, **23**, 399–410.

Dziewonski, A. M., 1977. Finite strain model of the Earth with consideration of velocity dispersion, *EOS Trans. Am. geophys. Un.*, **58**, 439.

Dziewonski, A. M. & Gilbert, F., 1972. Observations of normal modes from 84 recordings of the Alaskan earthquake of 1964 March 28, *Geophys. J. R. astr. Soc.*, **27**, 393–446.

Dziewonski, A. M. & Gilbert, F., 1974. Temporal variation of the seismic moment tensor and the evidence of precursive compression for two deep earthquakes, *Nature*, **247**, 185–188.

Dziewonski, A. M., Hales, A. L. & Lapwood, E. R., 1975. Parametrically simple earth models consistent with geophysical data, *Phys. Earth planet. Int.*, **10**, 12–48.

Gaulon, R., 1971. Observations des oscillations propres sphéroidales et toroidales, *Ann. Geophys.*, **27**, 141–149.

Gilbert, F., 1971. Ranking and winnowing gross earth data for inversion and resolution, *Geophys. J. R. astr. Soc.*, **23**, 125–128.

Gilbert, F. & Dziewonski, A. M., 1975. An application of normal mode theory to the retrieval of structural parameters and source mechanisms from seismic spectra, *Phil. Trans. R. Soc. Lond. A.*, **278**, 187–269.

Hart, R. S., Anderson, D. L. & Kanamori, H., 1977. The effect of attenuation on gross earth models, *J. geophys. Res.*, **82**, 1647–1654.

Jackson, D. D., 1971. The attenuation of Love waves and toroidal oscillations of the Earth, *Geophys. J. R. astr. Soc.*, **25**, 25–34.

Jobert, N. & Roult, G., 1976. Periods and damping of free oscillations observed in France after sixteen earthquakes, *Geophys. J. R. astr. Soc.*, **45**, 155–176.

Jordan, T. H. & Sipkin, S. A., 1977. Estimation of the attenuation operator for multiple ScS waves, *Geophys. Res. Lett.*, **4**, 167–170.

Kanamori, H., 1970. Velocity and Q of mantle waves, *Phys. Earth planet. Int.*, **2**, 259–275.

Kovach, R. L. & Anderson, D. L., 1964. Attenuation of shear waves in the upper and lower mantle, *Bull. seism. Soc. Am.*, **54**, 1855–1864.

Lee, W. B. & Solomon, S. C., 1978. Simultaneous inversion of surface wave phase velocity and attenuation: Love waves in western North America, *J. geophys. Res.*, in press.

Liu, H.-P., Anderson, D. L. & Kanamori, H., 1976. Velocity dispersion due to anelasticity: implications for seismology and mantle composition, *Geophys. J. R. astr. Soc.*, **47**, 41.

MacDonald, G. J. F. & Ness, N., 1961. A study of the free oscillations of the Earth, *J. geophys. Res.*, **66**, 1865–1912.

Mendiguren, J., 1973. High resolution spectroscopy of Earth free oscillations knowing the earthquake source mechanism, *Science*, **179**, 179–180.

Ness, N. F., Harrison, J. C. & Slichter, L. B., 1961. Observations of the free oscillations of the Earth, *J. geophys. Res.*, **66**, 621–629.

Nowroozi, A. A., 1968. Measurement of Q values from the free oscillations of the Earth, *J. geophys. Res.*, **73**, 1407–1415.

Nowroozi, A. A., 1974. Characteristic periods and Q for oscillations of the Earth following an intermediate focus earthquake, *J. Phys. Earth*, **22**, 1–23.

Reiter, L., 1973. Reflection, refraction, and mode conversion of long period surface waves and the measurement of Q^{-1} for free oscillations, *Bull. seism. Soc. Am.*, **63**, 1709–1722.

Roult, G., 1974. Attenuation des ondes sismiques de très basse frequence, *Ann. Geophys.*, **30**, 141–167.

Roult, G., 1975. Attenuation of seismic waves of very low frequency, *Phys. Earth planet. Int.*, **10**, 159–166.

Sailor, R. V. & Dziewonski, A. M., 1976. Attenuation of shear energy in the mantle from normal mode analysis, *Semiannual technical summary*, MIT Lincoln Laboratory, 1975 December 31, pp. 23–25, 33–37.

Slichter, L. B., 1967a. Spherical oscillations of the Earth, *Geophys. J. R. astr. Soc.*, **14**, 171–177.

Slichter, L. B., 1967b. Free oscillations of the Earth, in *Dictionary of geophysics*, Vol. I, pp. 331–343, ed. Runcorn, S. K., Pergamon, London.

Slichter, L. B., MacDonald, G. J. F., Caputo, M. & Hager, C. L., 1966. Comparison of spectra for spheroidal modes excited by the Chilean and Alaskan quakes, *Geophys. J. R. astr. Soc.*, **11**, 256.

Smith, S. W., 1961. An investigation of the Earth's free oscillations, *PhD thesis*, California Institute of Technology, Pasadena, California, USA.

Smith, Stewart W., 1972. The anelasticity of the mantle, *Tectonophys.*, **13**, 601–622.

Stein, S. & Geller, R. J., 1977. Split spheroidal and torsional mode studies of Q and the source mechanism and moment of the 1960 Chilean and 1964 Alaskan earthquakes, *EOS Trans. AGU*, **58**, 440.

Vaisnys, J. R., 1968. Propagation of acoustic waves through a system undergoing phase transformations, *J. geophys. Res.*, **73**, 7675–7683.

Wiggins, R. A., 1972. The general linear inverse problem: implications of surface waves and free oscillations for Earth structure, *Rev. Geophys. Space Phys.*, **10**, 251–285.

Wiggins, R. A. & Miller, S. P., 1972. New noise reduction technique applied to long-period oscillations from the Alaskan earthquake, *Bull. seism. Soc. Am.*, **62**, 471–479.